Direct Urea Fuel Cells

International Edition: DOI: 10.1002/anie.201606313
German Edition: DOI: 10.1002/ange.201606313

Metallic Nickel Hydroxide Nanosheets Give Superior Electrocatalytic Oxidation of Urea for Fuel Cells

Xiaojiao Zhu, Xinyu Dou, Jun Dai, Xingda An, Yuqiao Guo, Lidong Zhang, Shi Tao, Jiyin Zhao, Wangsheng Chu, Xiao Cheng Zeng, Changzheng Wu, and Yi Xie*

Abstract: *The direct urea fuel cell (DUFC) is an important but challenging renewable energy production technology, it offers great promise for energy-sustainable developments and mitigating water contamination. However, DUFCs still suffer from the sluggish kinetics of the urea oxidation reaction (UOR) owing to a 6 e^- transfer process, which poses a severe hindrance to their practical use. Herein, taking β-$Ni(OH)_2$ nanosheets as the proof-of-concept study, we demonstrated a surface-chemistry strategy to achieve metallic $Ni(OH)_2$ nanosheets by engineering their electronic structure, representing a first metallic configuration of transition-metal hydroxides. Surface sulfur incorporation successfully brings synergetic effects of more exposed active sites, good wetting behavior, and effective electron transport, giving rise to greatly enhanced performance for UOR. Metallic nanosheets exhibited a much higher current density, smaller onset potential and stronger durability.*

Driven by growing concerns about global warming and the depletion of fossil fuel, developing renewable energy-production and -storage technologies represent an important but challenging issue.[1–3] In this regard, direct urea fuel cells offer great promise for energy-sustainable developments and also mitigating water contamination.[4–6] The urea fuel cell is designed based on $2\,CO(NH_2)_2 + 3\,O_2 \rightarrow 2\,N_2 + 4\,H_2O + 2\,CO_2$, accomplishing power output and concurrently remedying urea-rich wastewater before urea naturally hydrolyzes in the environment. Compared to cathodic oxygen reduction reaction (ORR), the anodic urea oxidation reaction (denoted as UOR, $CO(NH_2)_2 + 6\,OH^- \rightarrow N_2 + 5\,H_2O + CO_2 + 6\,e^-$) undergoes more sluggish kinetics owing to a $6\,e^-$ transfer process and requires the use of electrocatalysts for promoting the reaction rate. Therefore, high-performance UOR catalysts are required to reduce the overpotential to drive the sluggish reaction. Although tremendous efforts have been devoted to pursue efficient electrocatalysts to give superior UOR performance,[7–15] they still suffer from inferior electrical conductivity and "poisoning", greatly hindering electrochemical efficiency for practical application.

Conductive two-dimensional (2D) nanosheets have been explored for high-performance electrocatalysts because of their highly exposed catalytic surface and excellent electron transportation. Two-dimensional nanomaterials usually possess exposed surfaces with low-coordinated steps, edges, and kinks, which provide abundant active sites to mediate the electrocatalytic process, allowing them to be efficient electrocatalysts.[16] Owing to the dimensionally reduced structure of 2D nanomaterials, in which most of atoms are exposed on surface and thus offer high chemical activity, various strategies directed at the surface atoms, including defect engineering, surface incorporation and structural distortion,[17–19] have been employed to effectively augment the number of active sites. Moreover, intrinsic high conductivity is also essential for improving electrocatalytic performances. A vast array of highly conductive 2D nanomaterials, spanning from transition-metal carbides Mo_2C,[20] nitrides Ni_3N,[21] phosphide Ni_5P_4-Ni_2P[22] to transition-metal dichalcogenides (TMD) 1T-WS_2,[23] benefit from abundant active sites and enhanced conductivity, consequently exhibiting superior electrocatalytic performance. However, for the urea-oxidation reaction (UOR) process, conductive 2D nanomaterials have been rarely used.[10,15] An open question is how to synergistically enhance electrical conductivity and regulate the active sites towards optimizing UOR electrocatalytic performance?

Herein, taking β-$Ni(OH)_2$ nanosheets as a proof-of-concept study, we demonstrated a surface-chemistry strategy to achieve a metallic phase of $Ni(OH)_2$ nanosheets by manipulating their electronic structure, representing the first metallic case among transition-metal hydroxides. Surface sulfur incorporation successfully brings synergetic effects of more exposed active sites by prohibiting the "poisoning" process, good wetting behaviors, and effective electron transport, giving rise to greatly enhanced performance for UOR. Metallic nanosheets exhibited a much higher current density, smaller onset potential, and higher stability. This work shed

[*] X. J. Zhu, X. D. An, Y. Q. Guo, J. Y. Zhao, Prof. C. Z. Wu, Prof. Y. Xie
Hefei National Laboratory for Physical Sciences at the Microscale
iChEM (Collaborative Innovation Center of Chemistry for Energy Materials), CAS Center for Excellence in Nanoscience, and CAS Key Laboratory of Mechanical Behavior and Design of Materials
University of Science & Technology of China
Hefei 230026 (P.R. China)
E-mail: czwu@ustc.edu.cn
X. Y. Dou
College of Chemistry, Jilin University
2699 Qianjin Street, Changchun, 130012 (China)
J. Dai, Prof. X. C. Zeng
Department of Chemistry, University of Nebraska-Lincoln
Lincoln, NE 68588 (USA)
Prof. L. D. Zhang
National Synchrotron Radiation Laboratory
University of Science and Technology of China
Hefei, Anhui 230029 (P.R. China)
S. Tao, Prof. W. S. Chu
National Synchrotron Radiation Laboratory
University of Science and Technology of China
Hefei, Anhui 230029 (P.R. China)

Supporting information for this article can be found under: http://dx.doi.org/10.1002/anie.201606313.

light on designing highly efficient electrocatalysts for energy conversion.

To enable effective sulfur incorporation, pristine $Ni(OH)_2$ (P-$Ni(OH)_2$) nanosheets were treated with an H_2S flow as the sulfur source at elevated temperature (Figure 1 a,b). Sulfur-incorporated $Ni(OH)_2$ products with a gradient of sulfur contents were selectively controlled at different reaction temperatures of 100 °C and 130 °C for 1 h (details in the Supporting Information). In our case, products acquired at 100 °C and 130 °C are denoted as S-$Ni(OH)_2$ and M-$Ni(OH)_2$, respectively. The ultrathin nature of the $Ni(OH)_2$ nanosheets obtained (Figure S2 in the Supporting Information) offers a structural platform with exposed surface atoms to facilitate the sulfur incorporation reaction. As a matter of fact, experimental (Figure S3, Movie S1) and theoretical investigations (Figure 1 c and Figure S4) indicate high feasibility for sulfur incorporation. Characterizations confirm that the original structure is maintained after surface chemical treatment. The X-ray powder diffraction (XRD) gives evidence that the long-range order of $Ni(OH)_2$ is preserved after the sulfur incorporation (Figure S5). X-ray absorption fine structure (XAFS) measurements, which are sensitive to local atomic and electronic structures, were performed to probe the local structure of three $Ni(OH)_2$ samples. The $k^2\chi(k)$ oscillation curve in Figure 2 a for S-$Ni(OH)_2$ and M-$Ni(OH)_2$ nanosheets have a spectral shape similar to that of P-$Ni(OH)_2$ nanosheets, which is accounted for by the preservation of the $Ni(OH)_2$ structure. In Figure 2 b, the Fourier transform curve of pristine $Ni(OH)_2$ nanosheets displays two peaks at approximately 1.86 Å and 2.99 Å, which can be attributed to Ni-O and Ni-Ni correlations, respectively. For S-$Ni(OH)_2$ nanosheets and M-$Ni(OH)_2$ nanosheets, the intensities of these two peaks are significantly decreased. Furthermore, Ni-O(S) peak for M-$Ni(OH)_2$ nanosheets is also accompanied with a noticeable shift (amplified in inset of Figure 2 b, and shift trend is indicated with a pink arrow) in position of the Ni-O peak towards high-R side, which can be ascribed to the larger atomic radius of S over O and in turn confirms sulfur incorporation into P-$Ni(OH)_2$ nanosheets. As described above, in spite of sulfur incorporation in $Ni(OH)_2$ structure, the pristine lattice framework was well maintained, verifying our structural model of sulfur substitution of oxygen atoms.

Employing element analyses upon isolated nanosheets give consistent results of sulfur incorporation into pristine $Ni(OH)_2$ framework. Elemental mapping performed on the M-$Ni(OH)_2$ nanosheet demonstrates that sulfur is homogeneously distributed on the nanosheet (Figure S6). In addition, the corresponding electron energy-loss spectrum (EELS) which shows sulfur L-edge from the core in Figure S7,[24] resembles that of MoS_2 and further confirms sulfur incorporation into

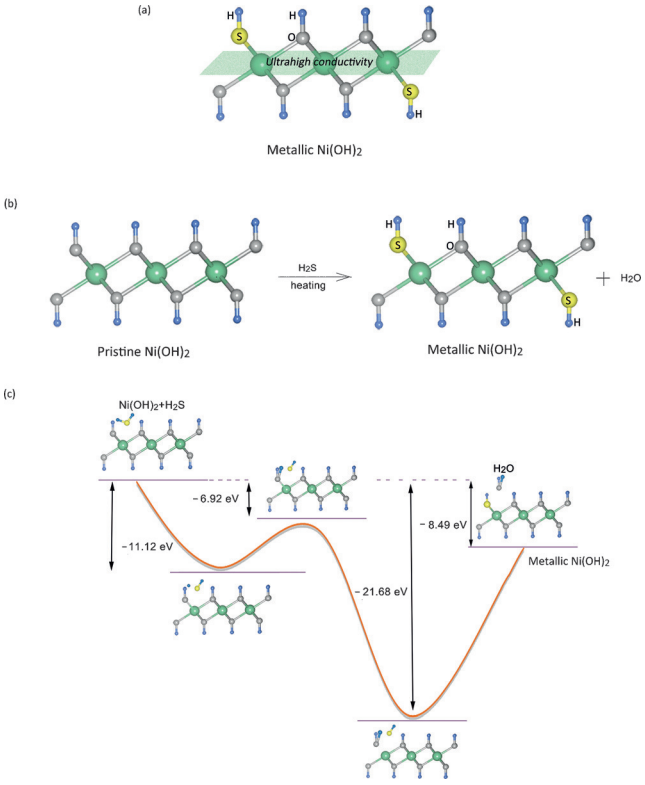

Figure 1. Schematic illustration of the sulfur incorporation into $Ni(OH)_2$ nanosheets resulting in metallic $Ni(OH)_2$ nanosheets. a) side view of the metallic $Ni(OH)_2$ nanosheets; b) schematic illustration of the reaction between H_2S and $Ni(OH)_2$ nanosheets; c) kinetics of the sulfur incorporation reaction.

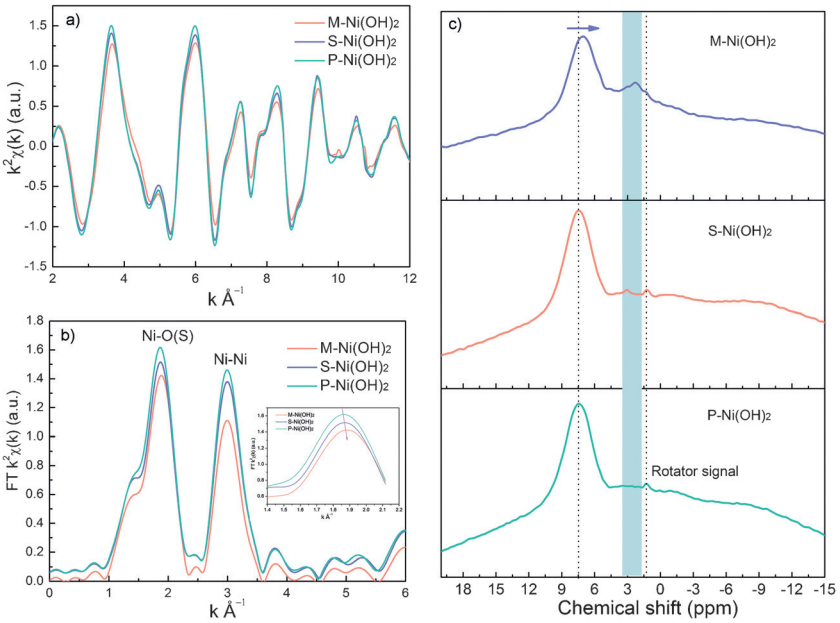

Figure 2. Sulfur incorporation into the pristine $Ni(OH)_2$ framework (P-$Ni(OH)_2$). a) Ni *K*-edge XAFS oscillation function $k^2\chi(k)$ and b) the corresponding Fourier transforms FT($k^2\chi(k)$), where k = wave vector and $\chi(k)$ = oscillation as a function of the photoelectron wavenumber; inset: zoomed-in view of Fourier transforms. c) ^{1}H solid-state MAS NMR spectra of the three $Ni(OH)_2$ samples. See text for details.

the $Ni(OH)_2$ nanosheets. The introduced -S–H group could be revealed by 1H solid-state MAS NMR spectra. As shown in Figure 2c, the strongest signals at around $\delta = 7.5$ ppm of the three samples are assigned to -O–H group, and downfield shift of the -O–H group signal in the spectra of M-$Ni(OH)_2$ nanosheets to $\delta = 7$ ppm can be attributed to prominent enhancement of electron density around H atoms triggered by the sulfur incorporation (the increment of electron concentration is discussed below). The -S–H entity is confirmed with the signals at around $\delta = 3$ ppm in the spectra of S-$Ni(OH)_2$ and M-$Ni(OH)_2$ nanosheets.[25] The blue rectangle area in Figure 2c is to highlight the content evolution of the -HS entity, while no -S–H characteristic peak is observed in the P-$Ni(OH)_2$ nanosheets. Similarly, signal of -S–H in the M-$Ni(OH)_2$ nanosheets is broadened and even expanded to high field compared to that of S-$Ni(OH)_2$ nanosheets, which can also be ascribed to prominent enhancement of electron density around H atoms. Therefore, incorporated sulfur in the form of -S–H groups that are bonded to the Ni atoms in the O–Ni–O structure scaffold.

To further demonstrate whether sulfur incorporation can effectively change the electronic structure, Ni *K*-edge XANES spectra of M-$Ni(OH)_2$ nanosheets and P-$Ni(OH)_2$ nanosheets (Figure 3a) enable the chemical state and geometry structure of the two samples to be discerned. Clearly, the pre-edge feature A (Figure 3a) didn't change much; and the spectral features B (Figure 3a) didn't show energy shift, indicating the pristine $Ni(OH)_2$ framework was well preserved after sulfur incorporation. The main change that is observed between the two samples is a shift of absorption threshold to lower energy with sulfur incorporation. As displayed in the inset of Figure 3a, due to smaller electronegativity of sulfur compared to that of oxygen, the edge of M-$Ni(OH)_2$ nanosheets show a downshift, indicating an increase in the electron concentration in the M-$Ni(OH)_2$ nanosheets. Furthermore, XPS spectra of metallic and pristine nanosheets also verify the increment of the electron concentration (Figure S8). Given sulfur atoms have a larger atomic radius and a smaller electronegativity compared to that of oxygen atoms, sulfur incorporation would lead to weaker covalent bonding and delocalize immobilized electrons, providing the possibility to change the electronic structure. The sulfur concentration in metallic nanosheets is characterized to be approximately 4.44% (Figure S9). Furthermore, density function theory (DFT) helps the understanding of the electronic structure evolution after sulfur incorporation. As shown in Figure 3b, with the sulfur incorporation, the wide band gap in pristine $Ni(OH)_2$ nanosheets turn into zero band, demonstrating the sulfur incorporation gives rise to metallic $Ni(OH)_2$ nanosheets.

The electrical property measurements revealed metallic transportation behavior for M-$Ni(OH)_2$ nanosheets. As shown in Figure 3c, M-$Ni(OH)_2$ nanosheets showed increase of electrical resistivity as the temperature increased with $d\rho/dT > 0$, which is typical of metallic character. In this case, M-$Ni(OH)_2$ nanosheets had a resistivity of 3.13×10^{-4} Ω·m at room temperature, exhibiting ultrahigh conductivity. The Hall coefficient (R_H) measurements as shown in Figure 3d were performed to further understand the charge-transport properties in the M-$Ni(OH)_2$ nanosheets. The negative values of R_H at different temperatures for M-$Ni(OH)_2$ nanosheets indicate that the main carriers are electrons, which is significantly different from the previously reported transporting model for the pristine $Ni(OH)_2$ nanosheets.[26] Furthermore, the electron concentration of M-$Ni(OH)_2$ nanosheets is approximately 10^{20} cm^{-3}, verifying that the sulfur incorporated structure brings metallicity with ultrahigh conductivity.

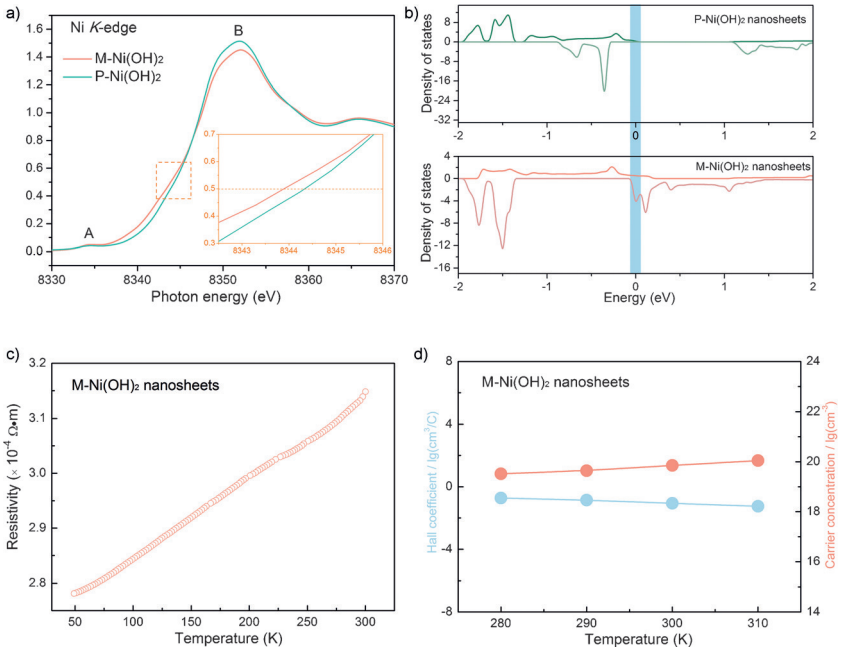

Figure 3. Electrical behavior regulation by sulfur incorporation in M-$Ni(OH)_2$ nanosheets. a) Ni *K*-edge XANES of M-$Ni(OH)_2$ nanosheets and P-$Ni(OH)_2$ nanosheets; inset: zoomed-in view of the Ni *K*-edge XANES. b) Density of states (DoS) of M-$Ni(OH)_2$ nanosheets and P-$Ni(OH)_2$ nanosheets (the vertical blue bar indicates the decrease in the bandgap after sulfur incorporation); c) Temperature-dependent resistivity of M-$Ni(OH)_2$ nanosheets; d) carrier concentration and Hall coefficient of M-$Ni(OH)_2$ nanosheets.

In our case, metallic nanosheets bring synergistic advantages of active sites ingrained in $Ni(OH)_2$ nanosheets as well as enhanced electrical conductivity, holding great promise for efficient UOR catalyst. To evaluate the UOR performance of metallic $Ni(OH)_2$ nanosheets, the linear sweep voltammetry (LSV) of M-$Ni(OH)_2$ catalyst deposited on glassy carbon electrode obtained in the absence and presence of 0.33 M urea in 1 M KOH solution at a scan rate of 50 $mV\,s^{-1}$, is shown in Figure 4a. As can be clearly seen, in 1 M KOH solution, at 0.344 V vs. Ag/AgCl, $Ni(OH)_2$ is oxidized to NiOOH. After the addition of urea, a significant increase on current density

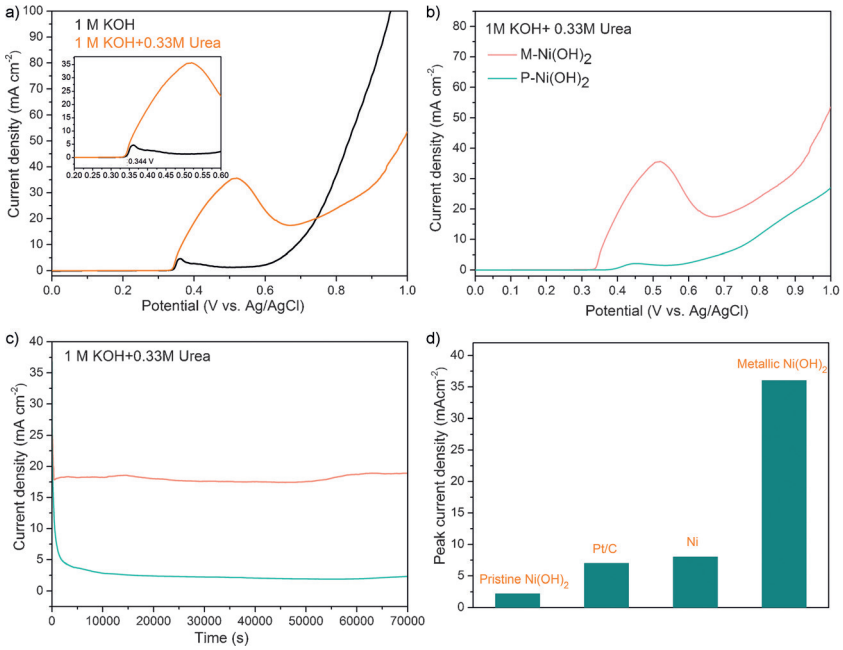

Figure 4. UOR catalytic properties of M-Ni(OH)$_2$ nanosheets. a) LSV plots of M-Ni(OH)$_2$ electrode in 1 M KOH, with and without 0.33 M urea, the inset shows the onset potential; b) LSV plots of the M-Ni(OH)$_2$ electrode and the P-Ni(OH)$_2$ electrode; c) Chronoamperometric response of the P-Ni(OH)$_2$ and the M-Ni(OH)$_2$ electrode in 1 M KOH + 0.33 M urea electrolyte at 0.46 V (vs. Ag/AgCl); d) peak current density comparison among different electrocatalysts.

with the onset potential at 0.344 V vs. Ag/AgCl was revealed. By contrast, the onset potential of metallic nanosheets is 28 mV smaller than that of pristine nanosheets (Figure S10). The onset potential of UOR is consistent with the potential where the NiOOH is formed, indicating that newly generated NiOOH species are active sites for urea oxidation, which have been investigated in detail in most of Ni-based electrocatalysts.[8–14]

Compared with pristine Ni(OH)$_2$ nanosheets, M-Ni(OH)$_2$ nanosheets deliver superior UOR performance with a higher catalytic activity and stability. Specifically, as shown in Figure 4b, M-Ni(OH)$_2$ nanosheets deliver a much higher peak current density, which is almost all contributed by oxidation of urea, demonstrating a much higher UOR catalytic activity. The electrooxidation of urea on metallic nanosheets electrodes were further evaluated with constant voltage analysis in 1M KOH solution in the absence and presence of 0.33 M urea. According to oxidation peak potential of urea of pristine nanosheets, 0.46 V vs. Ag/AgCl was chosen as applied potential in the chronoamperometry measurement. As displayed in the Figure 4c, current density of M-Ni(OH)$_2$ nanosheets electrode increased gradually until it approached a peak value at 15000 s. Clearly, the M-Ni(OH)$_2$ electrode delivers constant and higher current density, indicating that M-Ni(OH)$_2$ are stable and active electrocatalysts for UOR. Furthermore, to demonstrate the superior UOR performance of metallic Ni(OH)$_2$ nanosheets, the comparison of peak current density among different electrocatalysts (Figure S11 and Figure S12) is shown in Figure 4d, demonstrating metallic Ni(OH)$_2$ nanosheets are among the most active electrocatalysts for UOR.[4]

Importantly, aside from the high conductivity, CO_2 "poisoning" catalysts also strongly influence the UOR performance, which demands effective means to facilitate CO_2 desorption from the catalyst surface.[8] As is known, UOR on Ni(OH)$_2$ catalysts in alkaline electrolyte involves following steps, [Eq. (1)–(3)][27–29]

$$6\,Ni(OH)_2 + 6\,OH^- \rightleftharpoons 6\,NiOOH + 6\,H_2O + 6\,e^- \quad (1)$$

$$6\,NiOOH + CO(NH_2)_2 + H_2O \rightarrow 6\,Ni(OH)_2 + N_2 + CO_2 \quad (2)$$

Net UOR reaction :

$$CO(NH_2)_2 + 6\,OH^- \rightarrow N_2 + 5\,H_2O + CO_2 + 6\,e^- \quad (3)$$

The rate-determining step in reaction (2) is the adsorbed CO_2 desorption from surface of active sites.[30] In our case, sulfur incorporation can effectively lower energy barrier for intermediates formation and thus effectively facilitate overall reaction rate, as verified by density function theory calculation. Figure 5 describes kinetics energy barrier profiles of the rate-determining step: $[R{\cdot}CO_2]_{ads} \rightarrow R + CO_2$. R and R′ stands for respective catalytic species in pristine and metallic nanosheets. As can be clearly seen, energy barrier for the breakage of interaction between CO_2 and surface active species in $[R{\cdots}CO_2]_{ads}$ is smaller than that in the P-Ni(OH)$_2$ nanosheets, suggesting it's more favorable for CO_2 desorption from the surface of catalytic species in M-Ni(OH)$_2$ nanosheets, and thus exposing more active sites open for the catalytic procedure. From this

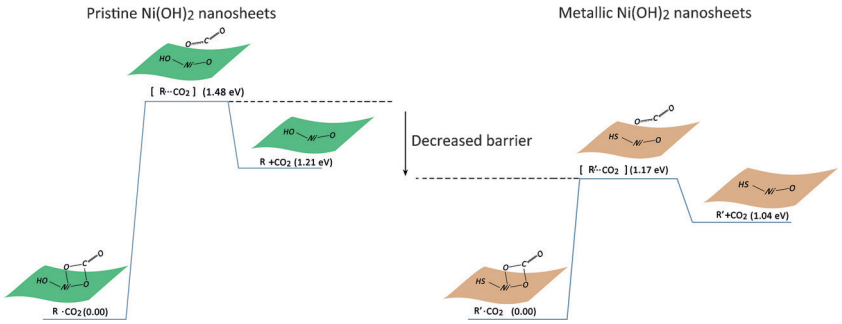

Figure 5. Kinetics for the CO_2 desorption from electrocatalysts surface. See text for details.

viewpoint, sulfur incorporation in metallic $Ni(OH)_2$ have the ability to effectively retard the "poisoning" of electrocatalysts, ensuring their superior UOR performance. Furthermore, sulfur incorporation did not compromise the inherent good wetting behaviors of pristine nanosheets, guaranteeing well-designed sulfur-incorporated structure competent with that of pristine nanosheets (Figure S13).

On the whole, metallic $Ni(OH)_2$ nanosheets deliver superior UOR performance, which benefit from synergistic effects: more exposed active sites by effectively inhibiting "poisoning" process; ultrahigh conductivity of $3.19 \times 10^3\ S\,m^{-1}$ at room temperature which ensures efficient charge transfer; together with good wetting behavior for good interfacial contact, demonstrating advances for highly efficient electrocatalysts for future application.

In conclusion, we demonstrate that surface sulfur modification is a way to successfully regulate the electronic structure in $Ni(OH)_2$ nanosheets, giving the first metallic case of 2D transition-metal hydroxide. The sulfur incorporation successfully accomplishes dual regulation of active sites and electrical behavior in metallic $Ni(OH)_2$ nanosheets. Metallic nanosheets deliver ultrahigh conductivity of $3.19 \times 10^3\ S\,m^{-1}$ at room temperature, ensuring effective electron transport; the Ni chemical state in the metallic nanosheets resulted in an accelerated CO_2 desorption rate from the surface of catalytic center and the consequent exposure of more active sites. Benefiting from synergistic effects of more exposed active sites, good wetting behaviors, and effective electron transport, metallic $Ni(OH)_2$ nanosheets deliver much enhanced UOR performance. Metallic nanosheets have a much higher current density, smaller onset potential, and greater stability than pristine $Ni(OH)_2$ nanosheets. This work provides an effective strategy to regulate the electrocatalytic performance of Ni-based structures.

Acknowledgements

This work was financially supported by the National Basic Research Program of China (2015CB932302), the National Natural Science Foundation of China (U1432133, 21501164, U1532265, 11321503, J1030412), the Chinese Academy of Sciences (XDB01020300), the Fok Ying-Tong Education Foundation, China (141042), and the Fundamental Research Funds for the Central Universities (WK2060190027, WK2340000065), National Program for Support of Top-notch Young Professionals, National Key Scientific Instruments and Equipment Development Program of China (2012YQ22011305).

Keywords: fuel cells · metallic transition-metal hydroxide · nanosheets · sulfur · urea oxidation reaction

How to cite: *Angew. Chem. Int. Ed.* **2016**, *55*, 12465–12469
Angew. Chem. **2016**, *128*, 12653–12657

[1] T. Lin, I. W. Chen, F. Liu, C. Yang, H. Bi, F. Xu, F. Huang, *Science* **2015**, *350*, 1508–1513.
[2] F. Bonaccorso, L. Colombo, G. Yu, M. Stoller, V. Tozzini, A. C. Ferrari, R. S. Ruoff, V. Pellegrini, *Science* **2015**, *347*, 1246501.
[3] M. Liu, R. Zhang, W. Chen, *Chem. Rev.* **2014**, *114*, 5117–5160.
[4] B. K. Boggs, R. L. King, G. G. Botte, *Chem. Commun.* **2009**, 4859–4861.
[5] G. Wang, Y. Ling, X. Lu, H. Wang, F. Qian, Y. Tong, Y. Li, *Energy Environ. Sci.* **2012**, *5*, 8215–8219.
[6] R. Lan, S. Tao, J. T. S. Irvine, *Energy Environ. Sci.* **2010**, *3*, 438–441.
[7] W. Xu, H. Zhang, G. Li, Z. Wu, *Sci. Rep.* **2014**, *4*, 5863.
[8] R. Lan, S. Tao, *J. Power Sources* **2011**, *196*, 5021–5026.
[9] D. Wang, W. Yan, S. H. Vijapur, G. G. Botte, *J. Power Sources* **2012**, *217*, 498–502.
[10] D. Wang, W. Yan, G. G. Botte, *Electrochem. Commun.* **2011**, *13*, 1135–1138.
[11] Y. Liang, Q. Liu, A. M. Asiri, X. Sun, *Electrochim. Acta* **2015**, *153*, 456–460.
[12] M.-S. Wu, R.-Y. Ji, Y.-R. Zheng, *Electrochim. Acta* **2014**, *144*, 194–199.
[13] R.-Y. Ji, D.-S. Chan, J.-J. Jow, M.-S. Wu, *Electrochem. Commun.* **2013**, *29*, 21–24.
[14] W. Yan, D. Wang, G. G. Botte, *Electrochim. Acta* **2012**, *61*, 25–30.
[15] S. Chen, J. Duan, A. Vasileff, S. Z. Qiao, *Angew. Chem. Int. Ed.* **2016**, *55*, 3804–3808; *Angew. Chem.* **2016**, *128*, 3868–3872.
[16] Y. Sun, S. Gao, F. Lei, Y. Xie, *Chem. Soc. Rev.* **2015**, *44*, 623–636.
[17] F. Lei, Y. Sun, K. Liu, S. Gao, L. Liang, B. Pan, Y. Xie, *J. Am. Chem. Soc.* **2014**, *136*, 6826–6829.
[18] J. Xie, J. Zhang, S. Li, F. Grote, X. Zhang, H. Zhang, R. Wang, Y. Lei, B. Pan, Y. Xie, *J. Am. Chem. Soc.* **2013**, *135*, 17881–17888.
[19] Y. Sun, Q. Liu, S. Gao, H. Cheng, F. Lei, Z. Sun, Y. Jiang, H. Su, S. Wei, Y. Xie, *Nat. Commun.* **2013**, *4*, 2899.
[20] F.-X. Ma, H. B. Wu, B. Y. Xia, C.-Y. Xu, X. W. Lou, *Angew. Chem. Int. Ed.* **2015**, *54*, 15395–15399; *Angew. Chem.* **2015**, *127*, 15615–15619.
[21] K. Xu, P. Chen, X. Li, Y. Tong, H. Ding, X. Wu, W. Chu, Z. Peng, C. Wu, Y. Xie, *J. Am. Chem. Soc.* **2015**, *137*, 4119–4125.
[22] X. Wang, Y. V. Kolen′ko, X.-Q. Bao, K. Kovnir, L. Liu, *Angew. Chem. Int. Ed.* **2015**, *54*, 8188–8192; *Angew. Chem.* **2015**, *127*, 8306–8310.
[23] D. Voiry, H. Yamaguchi, J. Li, R. Silva, D. C. B. Alves, T. Fujita, M. Chen, T. Asefa, V. B. Shenoy, G. Eda, M. Chhowalla, *Nat. Mater.* **2013**, *12*, 850–855.
[24] Y.-C. Lin, D. O. Dumcenco, Y.-S. Huang, K. Suenaga, *Nat. Nanotechnol.* **2014**, *9*, 391–396.
[25] M. Sardo, R. Siegel, S. M. Santos, J. Rocha, J. R. B. Gomes, L. Mafra, *J. Phys. Chem. A* **2012**, *116*, 6711–6719.
[26] A. Motori, F. Sandrolini, G. Davolio, *J. Power Sources* **1994**, *48*, 361–370.
[27] V. Vedharathinam, G. G. Botte, *Electrochim. Acta* **2012**, *81*, 292–300.
[28] V. Vedharathinam, G. G. Botte, *Electrochim. Acta* **2013**, *108*, 660–665.
[29] D. Wang, G. G. Botte, *ECS Electrochem. Lett.* **2014**, *3*, H29–H32.
[30] D. A. Daramola, D. Singh, G. G. Botte, *J. Phys. Chem. A* **2010**, *114*, 11513–11521.

Received: June 29, 2016
Published online: August 30, 2016

